



Granular crystals as strong and fully dense architected materials

Ashta Navdeep Karuriya^a and Francois Barthelat^{a,1}

Edited by David Weitz, Harvard University, Cambridge, MA; received September 12, 2022; accepted November 21, 2022

Dense topologically interlocked panels are made of well-ordered, stiff building blocks interacting mainly by frictional contact. Under mechanical loads, the deformation of the individual blocks is small, but they can slide and rotate collectively, generating high strength, toughness, impact resistance, and damage tolerance. Here, we expand this construction strategy to fully dense, 3D architected materials made of space filling building blocks or “grains.” We used mechanical vibrations to assemble 3D printed rhombic dodecahedral and truncated octahedral grains into fully dense face-centered cubic and body-centered cubic “granular crystals.” Triaxial compression tests revealed that these granular crystals are up to 25 times stronger than randomly packed spheres and that after testing, the grains can be recycled into new samples with no loss of strength. They also displayed a rich set of mechanisms: nonlinear deformations, crystal plasticity reminiscent of atomistic mechanisms, geometrical hardening, cross-slip, shear-induced dilatancy, and microbuckling. A most intriguing mechanism involved a pressure-dependent “granular crystal plasticity” with interlocked slip planes that completely forbid slip along certain loading directions. We captured these phenomena using a three-length scale theoretical model which agreed well with the experiments. Once fully understood and harnessed, we envision that these mechanisms will lead to 3D architected materials with unusual and attractive combinations of mechanical performances as well as capabilities for repair, reshaping, on-site alterations, and recycling of the building blocks. In addition, these granular crystals could serve as “model materials” to explore unusual atomic scale deformation mechanisms, for example, non-Schmid plasticity.

architected materials | topological interlocking | granular crystals | crystal plasticity | microbuckling

Architected materials and other mechanical metamaterials use slender and flexible microstructures to create and program nonlinearities, instabilities, or other unusual mechanical responses (1). Another class of architected materials is fully dense and made of relatively stiff and hard building blocks in the order of millimeters in size, exploiting frictional contact and topological interlocking to generate impact resistance and damage tolerance (2–4). In these “topologically interlocked materials” (TIMs), individual blocks have a tightly controlled geometry, and they are arranged in periodic arrays which can be assembled into panels using a variety of methods (5), including mechanical vibrations (6). TIMs can generate remarkable structural properties: Compared to monolithic plates of the same material, they can be not only up to 50× tougher but also up to 1.2× stronger (4). While these concepts are well developed for relatively thin structures such as flat panels, curved panels, domes, or walls, so far there have been few attempts to harness this construction strategy and mechanisms in fully 3D materials (7, 8). Interestingly, granular materials share some of the key characteristics of TIMs since they are also made of millimeter-size building blocks interacting by frictional contact, albeit in full three dimensions. Granular materials like sand display a wide range of complex mechanical responses that have so far not been exploited in TIMs. For example, depending on confinement, sand can flow like a liquid or be as stiff and strong as a solid (9), with a rich set of mechanisms that include the formation of clusters, localized regions of stress transfer, jamming, shear bands, and shear-induced dilatation (10, 11). Randomness in typical granular packings makes it however difficult to design, optimize, and exploit these deformation mechanisms for broader engineering applications. In addition, granular materials are usually based on spherical or ellipsoidal grains (10, 11), which in terms of mechanical performance spherical shapes are suboptimal: The packing factor (solid volume fraction) for a random packing of spheres is only 0.55 to 0.64 (12), which is significantly smaller than the upper bound volume fraction in closed packed spheres (0.74), which itself is much lower than 1 because spheres are not space-filling shapes. As a result, mechanical loads applied to typical granular materials are channeled along thin “force chains” that occupy only a small fraction in the material (13), while most grains remain free of stress. The mechanical response of

Significance

Topologically interlocked materials display an unusual and interesting combination of mechanical properties but only in panel or other relatively thin 2D structures. Here, we expand this concept to 3D, with nearly fully dense “granular crystals” at the intersection of architected materials and granular materials. These materials are up to 25 times stronger than traditional granular materials and have a rich set of deformation mechanisms: microbuckling, granular crystal plasticity, and geometrical hardening. These properties and mechanisms emerge from the geometry of individual grains, their crystallinity, and their orientation. These granular crystals can be used as modular structural materials that could be built from “universal” building blocks and that could be easily repaired and recycled.

Author affiliations: ^aDepartment of Mechanical Engineering, University of Colorado, Boulder, CO 80309

Author contributions: A.N.K. and F.B. designed research, performed research, contributed new reagents/analytic tools, analyzed data, and wrote the paper.

The authors declare no competing interest.

This article is a PNAS Direct Submission.

Copyright © 2022 the Author(s). Published by PNAS. This article is distributed under [Creative Commons Attribution-NonCommercial-NoDerivatives License 4.0 \(CC BY-NC-ND\)](https://creativecommons.org/licenses/by-nc-nd/4.0/).

¹To whom correspondence may be addressed. Email: francois.barthelat@colorado.edu.

This article contains supporting information online at <https://www.pnas.org/lookup/suppl/doi:10.1073/pnas.2215508120/-/DCSupplemental>.

Published December 27, 2022.

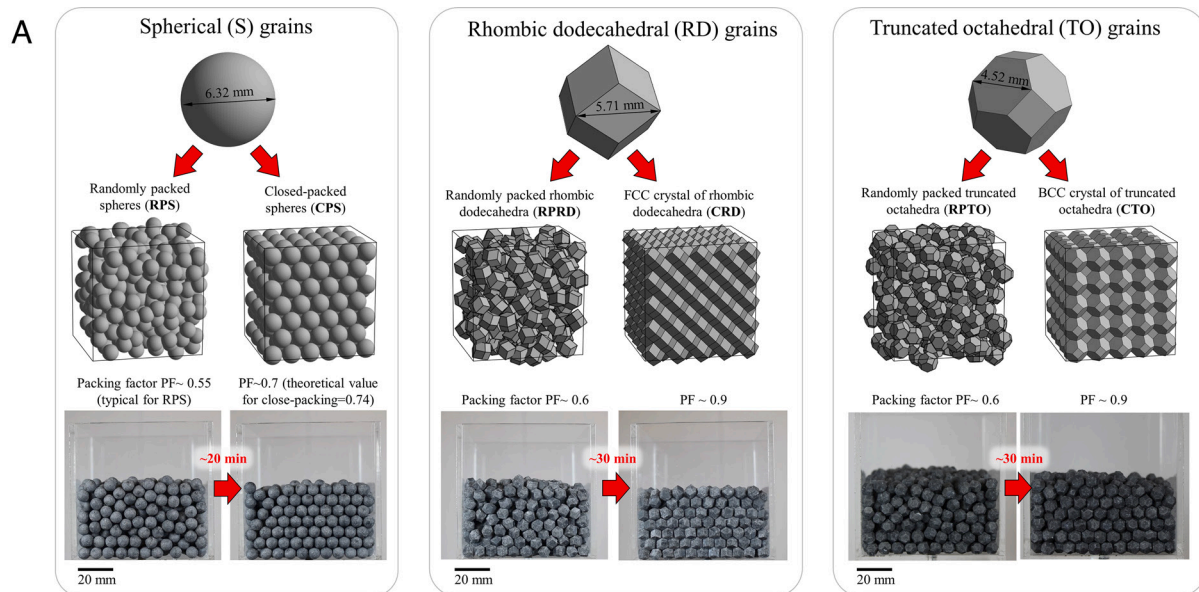
one-dimensional granular chains (14, 15) and granular crystals based on spherical grains (16) in small deformation regimes display unusual and useful characteristics in terms of elastic wave propagation, acoustics, or shock waves attenuation. Interestingly, the shape of the individual grains can also be designed to manipulate mechanical responses and enhance properties (17, 18). For example, granular materials based on convex platonic shapes (cubes, tetrahedra, and octahedra) show a 40 to 80% increase of shear strength compared to materials based on spherical grains because of limited grain rotation and enhanced jamming (19). The arrangement of these grains is however random, which still limits their packing density and mechanical properties. A possible way to increase strength is to induce crystallization of the grains, which can improve packing factor and enhance load transfer in the material. Crystallization can be induced with combinations of particle shape, interaction forces, and compaction protocol (20) (21). Complex 3D granular crystals have been created but so far mostly at submicron scales where entropic forces and thermal agitation are significant [“colloidal lattices” (22, 23)]. Materials that would combine the concepts of TIMs, granular mechanics, and 3D crystallization could open new directions in material design that have so far not been explored. In this report, we present the design, fabrication, and mechanical testing of nearly fully dense “granular crystals” with millimeters-size grains, which expand some of the concepts of TIMs to three dimensions while borrowing some characteristics from granular materials. We first present our fabrication methods and mechanical testing, and then, we present a three-length scale mechanical model that captures the micromechanics of deformation in the granular crystals.

Results and Discussion

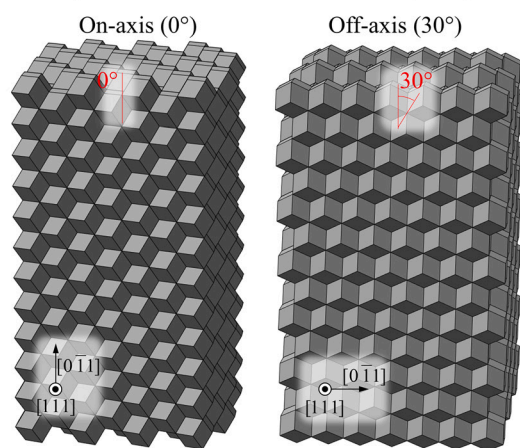
For this study, we considered grains in the shape of rhombic dodecahedra (RD), which is an attractive geometry because in theory, this polyhedron tessellates space in a face-centered, fully dense cubic (FCC) crystalline structure. We also considered truncated octahedra (TO), which tessellates space in a body-centered cubic (BCC) crystalline structure. These configurations can also be understood by considering 3D Voronoi tessellations computed from seeds on periodic 3D lattices. Individual Voronoi cells computed from seeds on a FCC lattice are RD, and Voronoi cells on a BCC lattice are TO. By way of the Voronoi construction, these regular shapes naturally tessellate space according to prescribed types of lattices. For reference, we also fabricated and tested granular materials based on spheres since they are common in granular mechanics (24). The fabrication of individual grains was carried out with a high-resolution 3D printer based on digital light processing (DLP, EnvisionTEC Micro HiRes). This printing method can produce individual grains which are fully dense, isotropic, and with a smooth surface comparable to injection molding. We used an ABS-like photocurable material, which is relatively stiff (measured Young’s modulus $E_g = 3$ GPa) and strong (measured yield strength = 70 MPa), with a measured friction coefficient $f^{(g)} = 0.30 \pm 0.05$ (SI Appendix). Importantly, the dimensions of the individual grains (Fig. 1A) were chosen so their volume was held constant ($V_g = 132$ mm³) for all grain geometries. The granular systems we considered contained $N = 800$ grains each, which occupied an approximate volume of $50 \times 40 \times 80$ mm³ (with some variations depending on the packing factor). Finally, for each grain geometry, we considered a random packing and a crystallized packing. Granular crystals were created by placing the grains in a rectangular container which was then subjected to high amplitude vibrations (amplitude = 4 mm, frequency = 18 Hz). Although we do not fully

understand the mechanisms of crystallization yet and why these vibration parameters are optimum, observations on the assembly process (SI Appendix, Movies S1) suggest that the energy provided by the mechanical vibrations must be high enough to “toss” individual grains and bounce neighboring grains beyond their exclusion volume so they can move, rotate, and find their crystallized position of minimal energy. Within about 20 to 30 min of applied vibrations, the grains assembled into large 3D single granular crystals (Fig. 1B) that approached the theoretical packing factor (PF) for spheres (PF ~ 0.7), for RD (PF > 0.91), and for TO (PF > 0.91). The nonplanar surfaces of the granular samples did not perfectly conform to the flat walls of the assembly box, which had a nonnegligible effect on the measured PF. The measured PF reported here can therefore be interpreted as lower bound for the actual PF for the granular crystals. Interestingly, the walls of the container also acted as templates in the crystallization process, a phenomenon also observed in traditional granular materials (24). For our FCC granular crystals, the {111} plane, which the plane of densest granular packing, always aligned with the floor of the assembly box. The side walls also played a role in templating the crystal: The three $\langle 110 \rangle$ directions within the {111} plane are the directions of densest linear packing for the grains, and this direction aligned either with the long vertical walls of the box, which created an “on-axis orientation,” or with the short vertical walls of the box, which created an “off-axis orientation” (Fig. 1B). The assembly box could therefore be used to control the texture of the crystal. We obtained similar results when we assembled BCC granular crystals (Fig. 1C), with the {110} plane parallel to the floor of the assembly box, and the side walls creating either an on-axis or off-axis alignment (Fig. 1C).

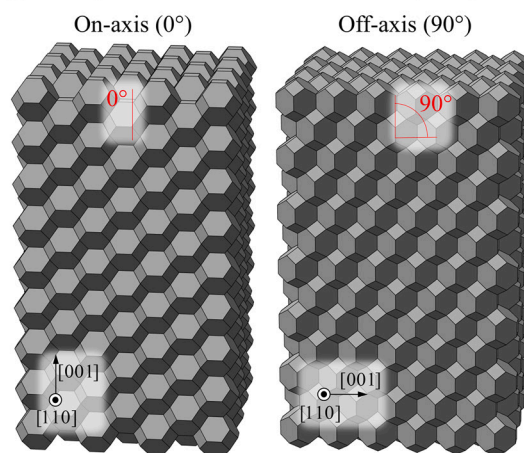
The orientation of the crystal had profound implications on the deformation mechanism and strength in the crystal when compressed along the long axis of the sample, as detailed in the next sections. Finally, we devised a protocol to crystallize the grains in a vacuum bag made of a 63-micron thick polypropylene film so that the crystallized samples could be easily handled and transferred to a universal testing machine (ADMET eXpert 5603) for compression tests along their long axis (Fig. 1D and E). During the test, vacuum was regulated to maintain one of three levels of confinements: $p_0 = 10$ kPa, $p_0 = 30$ kPa, or $p_0 = 60$ kPa. The air pressure in the vacuum bag was applied to all faces of each grain in a hydrostatic fashion so that it had no effect on grain motion. In contrast, the outer atmospheric pressure was first transferred to the outer grains through the vacuum bag and then transferred to the volume of the grains through direct contact between grains. We verified experimentally that the deformations and stresses in the vacuum bag did not contribute to overall strength by replicating some of the tests using thinner bags. Indeed, within the limits of thin membrane approximation for the bag, a simple mechanical model (SI Appendix, Fig. S3) shows that the mechanism of transfer of the confining pressure onto the grains does not depend on the contact area between the grains and the membrane, is independent from the deflection of the membrane, and independent from the in-plane stiffness of the membrane. Interestingly, after each test, the grains could be recovered, recycled, and reassembled into new samples with no loss of overall strength. Fig. 2A and B shows stress–strain curves for randomly packed spheres (RPS) and for crystallized rhombic dodecahedra (CRD) tested along the on-axis loading direction (Movies S1 and S2). The compressive strength was higher for higher confining pressure, which is typical of granular materials and was expected since the grains interact by frictional contact. The randomly packed grains displayed the expected response, with a steady and relatively low flow stress (Fig. 2A). Modulus



B Crystallized Rhombic Dodecahedra (CRD)



C Crystallized Truncated Octahedra (CTO)



D

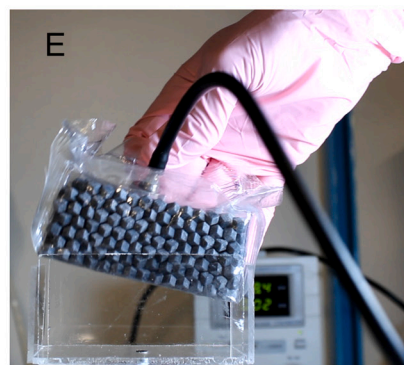
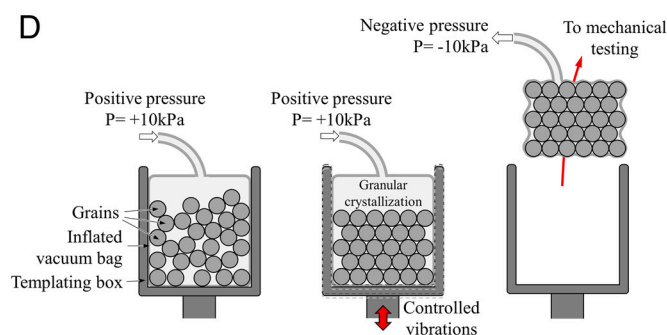


Fig. 1. Granular crystal design and fabrication: (A) We designed individual spherical, rhombic dodecahedral, and truncated octahedral grains in the millimeter scales so they have identical volumes. These grains can crystallize into close-packed spheres or fully dense FCC or BCC crystals, which we achieved experimentally using vibrations; interestingly, the box acted as a template for crystallization so that two distinct crystallographic orientations were obtained for (B) the crystallized rhombic dodecahedra (CRD) and (C) the crystallized truncated octahedra (CTO) samples; (D) we devised a protocol to crystallize the grains in a vacuum bag so they could (E) be transferred for mechanical testing.

and strength increased linearly with higher confinement, in a way which is consistent with the classical Mohr–Coulomb failure criterion with an internal frictional angle of about 35° (which is nearly identical to sand, see *SI Appendix, Fig. S2*). On the other extreme, in terms of material properties, the CRD granular crystals were 10 to 20 times stiffer and stronger than the randomly

packed grains with a stiff response and a peak stress at about 5 to 10% deformation followed by a sharp drop (Fig. 2B). Strength also increased with hydrostatic pressure, but this dependence did not follow the Mohr–Coulomb criterion (*SI Appendix, Fig. S2*). Unloading-reloading cycles (not shown here) showed that the sample tested deformed plastically in the nonlinear regions of the

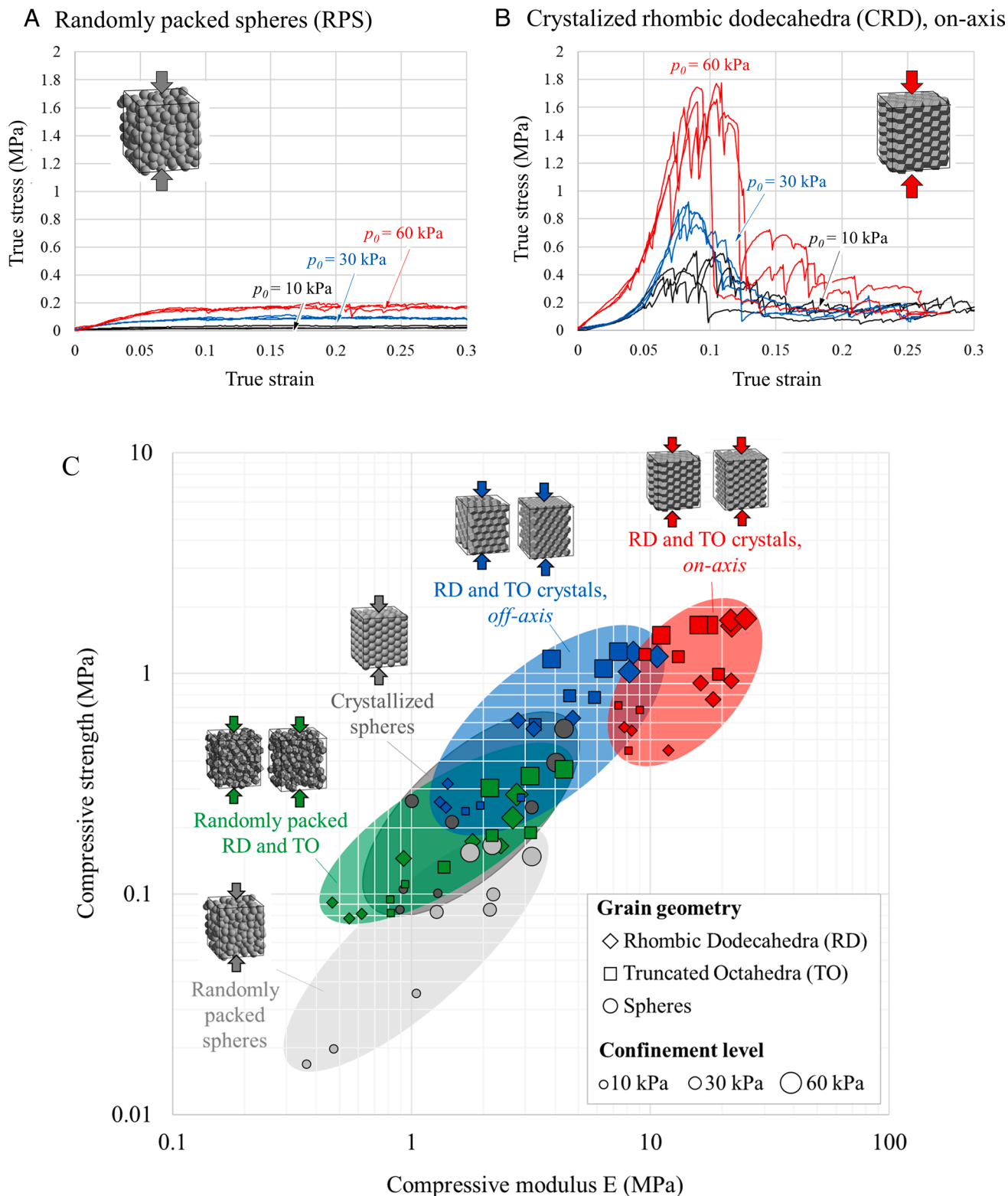


Fig. 2. Compressive stress–strain curve for (A) randomly packed spheres and (B) crystallized rhombic dodecahedral grains (on-axis). (C) Modulus–strength property chart for all materials tested in this study. The colors highlight the different arrangement and texture of the grains. The shape of the individual markers refers to the geometry of the individual grains, and the size of the markers refers to the level of confinement.

stress–strain curves. Other samples with different combinations of grains geometries and crystallinities produced a broad range of mechanical responses and properties, which are shown on the property map of Fig. 2C. This map shows a strong correlation between modulus and strength in these materials, and it also highlights the effects of grain geometry, of granular crystallinity,

and the synergistic effects between grain geometry and crystallinity. The effect of grain geometry can be observed on randomly packed samples: Randomly packed RD and TO materials were in the same range of stiffness as the RPS but 2 to 4 times stronger, a result consistent with previous experiments on randomly packed grains with tailored geometries (19). The effect of crystallization

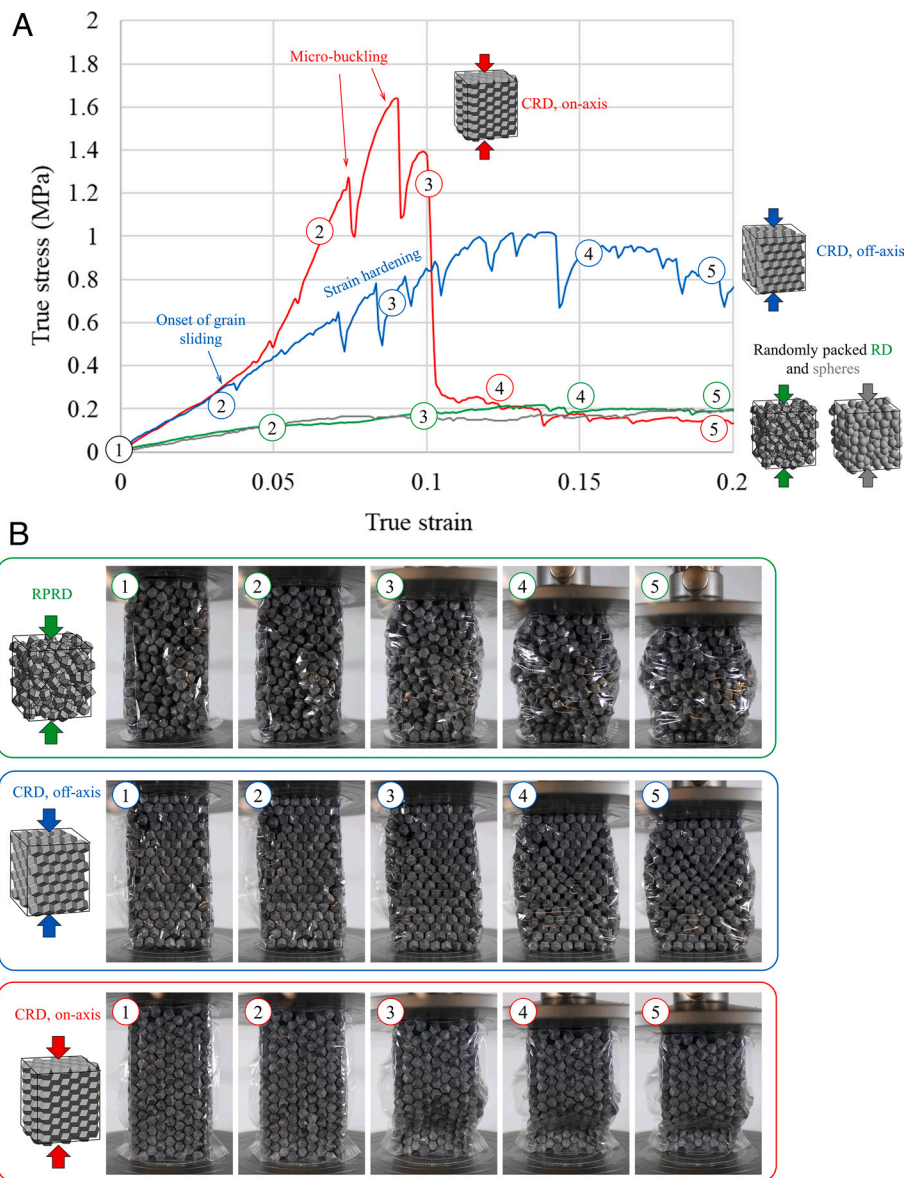


Fig. 3. Micromechanics of deformation: (A) compressive stress–strain curves for granular systems based on rhombic dodecahedral (RD) grains and at a confining pressure of $p_0 = 60$ kPa. Randomly packed RD grains have a response which is similar to randomly packed spheres (RPS) which is also shown. Crystallized samples show more complex responses that include peak stresses and softening; (B) Snapshots of the samples at different stage of compression reveal a broad range of mechanisms that include grain-on-grain sliding along slip planes, dilation, and microbuckling.

is also evident from the map, but the amplification of properties was more pronounced for the RD and TO granular materials compared to the sphere-based materials: Crystallized spheres were 2 to 4 times stronger than RPS for the same stiffness, while RD and TO based granular crystals were 2 to 17 times stiffer than their randomly packed counterparts and 3 to 7 times stronger (depending on confining pressure and crystal orientation). These observations show that improvements in stiffness and strength are produced by synergistic effects between grain geometry and granular crystallinity. These synergies give rise to significant improvements: The CRD and crystallized truncated octahedra (CTO) granular crystals materials are 6 to 15 times stiffer and 10 to 25 times stronger than RPS. The orientation of the crystal had an important effect on properties and deformation mechanisms, with the CRD and CTO crystals displaying the stiffest and strongest responses. The mechanical properties of crystals made of TO and RD were quite similar (the TO crystals were slightly stronger), although the deformation mechanisms were slightly different as elaborated below. Fig. 3 illustrates the different

deformation mechanisms we observed for RD-based materials with typical compressive stress–strain curves and snapshots of the samples for RD-based materials at a confining pressure of $p_0 = 60$ kPa. The randomly packed materials showed a typical response, with a relatively steady flow stress and homogenous “flow” of the grains. The CRD loaded along the on-axis direction did not slide or move significantly, with a “smooth” and relatively stiff response up to the peak stress, which was followed by a sharp decrease in stress. In this configuration, the grains form an array of parallel columns that carry the compressive force through flat-on-flat contacts, which produced a stiff and strong response. Imaging revealed that near the peak load columns of grains buckled collectively, leading to the rapid decrease in stress on the stress–strain curve. The CRD samples loaded along the off-axis direction deformed and failed in yet a completely different fashion: Granular “yielding” occurred along specific planes in the materials, in a way akin to atomic-scale crystal plasticity. Using an image tracking algorithm on individual grains (*SI Appendix*), we determined that the grains started to slide on one another at relatively

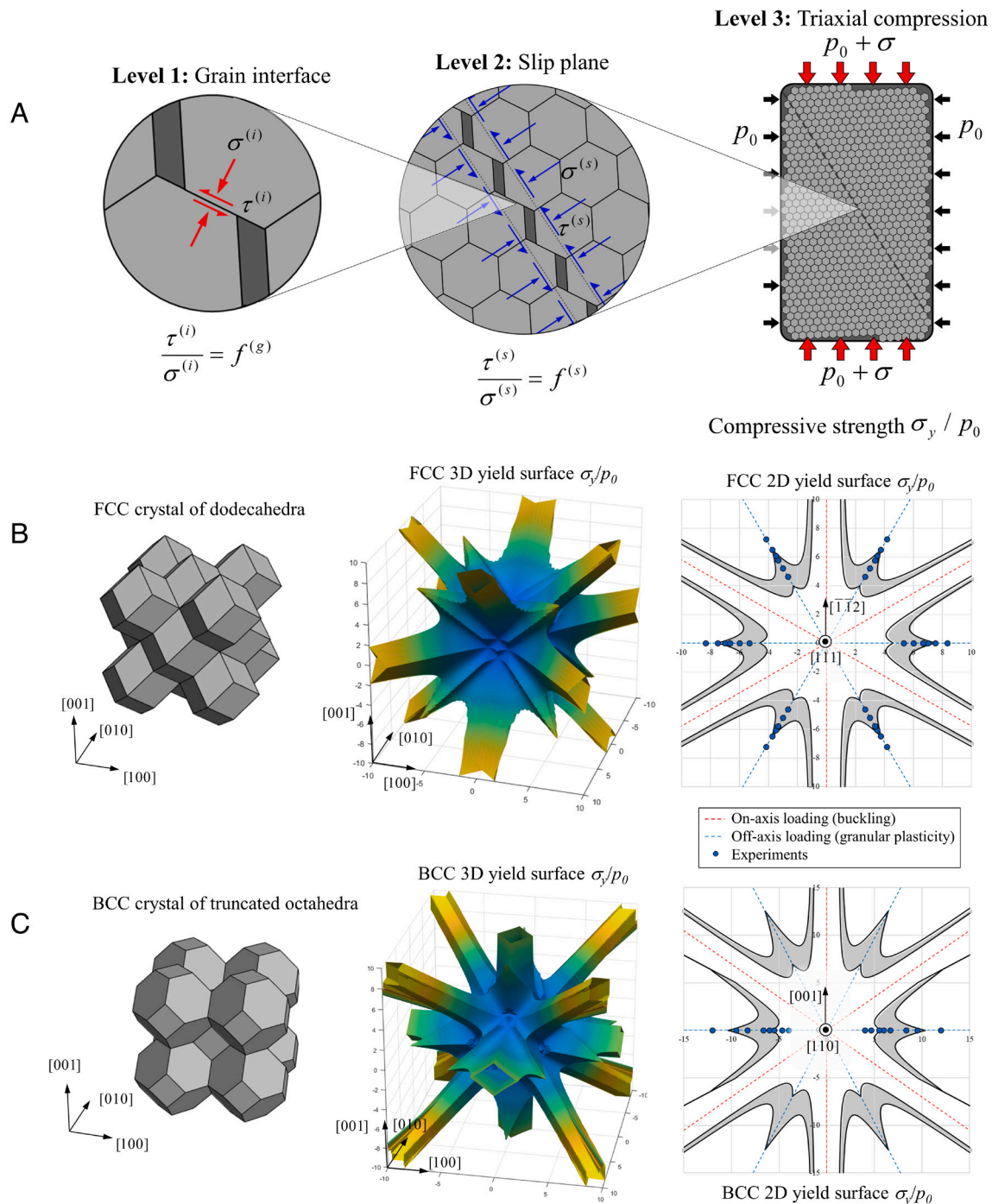


Fig. 4. A crystal plasticity model: (A) micromechanics of deformation can be captured with a three-level approach that incorporates friction between individual grains, friction of slip planes, resolved stresses, and slip plane activation depending on loading orientation; yield strength of (B) FCC and (C) BCC granular crystals predicted by this model. Since friction governs grain-to-grain interactions, the strength is written as σ_y/p_0 and can be displayed as 3D yield envelopes. (The surface was colored to highlight the directions of higher strength, in yellow.) Sections of these envelopes along the $\{111\}$ plane (FCC) and the $\{110\}$ plane (BCC) are also displayed, with the gray range of predictions corresponding to the model prediction based on the experimental range of grain-on-grain friction ($f^{(g)} = 0.30 \pm 0.05$). The model predicts forbidden directions for plasticity (and where buckling occurs) and agrees well with experimental strengths in the off-axis directions.

low stresses (0.1 to 0.4 MPa), corresponding to about 1/3 of the peak stress. The onset of granular yielding was followed by extensive strain hardening until a peak compressive stress followed by softening. Interestingly, grain sliding occurred along planes of densest packing in the crystals, in a way consistent with traditional crystal plasticity in FCC or BCC materials.

To capture this peculiar deformation mode, we developed a “granular crystal plasticity” model which captured the main mechanism of deformation over three-length scales (Fig. 4A; details are provided in *SI Appendix*). At the smallest scale (level 1),

grain-on-grain interactions are governed by frictional contact, with a simple Coulomb friction model with static coefficient of friction $f^{(g)}$. At level 2, we considered the possible slip systems within the crystals, consisting of the slip planes $\{111\}$ for FCC and $\{110\}$ for BCC, as well as partials (*SI Appendix*). We computed the effective friction $f^{(s)}$ for the slip planes, accounting for grain-on-grain friction, geometry of the slip plane interface, and slip direction within the slip plane. Because of the morphology of the slip plane that generates geometrical obstacles to sliding, as well as a strong directionality, we found that effective

slip plane friction $f^{(s)}$ is 3 to 5 times greater than grain-on-grain friction $f^{(g)}$, with a pronounced effect of the direction of slip within the slip plane. Finally at level 3, a hydrostatic compression p_0 was applied and superimposed with a uniaxial compression σ_a applied along a specific direction for the crystal. The resolved shear stress and resolved normal stress were computed on each available slip plane, and the condition for slip was applied to predict the compressive yield strength σ_y of the crystal. Fig. 4A shows the modeling approach in a 2D way, but the actual model captured the details of the geometry of the grains, crystallinity, morphology of the slip planes, and partials in three dimensions. We also considered a broad range of loading directions to explore the anisotropic response of the crystal. Importantly, since the entire process is governed by Coulomb friction, the strength of the crystal can be written in terms of the ratio σ_y/p_0 . Fig. 4 B and C shows that the strength of the crystal is strongly anisotropic and that there are loading directions where granular plasticity is simply forbidden. In these directions, the orientations and morphology of the slip planes are such that either the resolved shear on the slip plane is zero, or the grains interlock and prevent any slip. The only available failure mode in these directions is therefore buckling of the column of grains, as observed in the experiments on the on-axis samples. The model properly predicts that these strong directions match the faces of the individual grains in the crystal. In the FCC crystal made of 12-face RD, there are 6 strong directions where grains are interlocked, and the failure envelope has a 12-fold symmetry since the grains are regular polyhedra. In the BCC crystal made of 14-face TO, there are 7 strong directions, and the failure envelope has less symmetries because the grains have a nonregular geometry. In other loading directions, the model properly predicts the activation of one or more slip planes, which leads to a finite “yield strength” for the granular crystal. It is useful to consider cross-sections of these 3D failure envelopes along the $\{111\}$ plane for FCC and the $\{110\}$ for BCC since in the experiments, the compression is applied within these planes. These 2D projections show that the model is in excellent agreement with experiments on “off-axis” samples (Fig. 4 B and C). CTO crystals were slightly stronger because their slip planes are not truly closed packed, leading to higher slip plane coefficient of friction compared to the CRD (Fig. 4B). Finally, a striking feature in the off-axis experiments is the massive amount of strain hardening and spreading of deformations by slip in almost the entire volume of the sample. We explain this phenomenon with several mechanisms of geometrical hardening: increasing confinement due to grain climbing and dilation across the slip plane as well as cross slip and the formation of “steps” or geometrical obstacles on the slip planes. As the grains slide on one another, the contribution of hardening is however progressively offset by loss of contact area between the grains, and this competition gives rise to a maximum stress followed by a slow decay.

In summary, we have assembled and tested strong millimeter-size granular crystals which are up to 25 times stronger than regular granular materials. These 3D materials were directly inspired by 2D TIMs, and they share many of their characteristics: stiff building blocks assembled following spatial periodicity, controlled frictional sliding at the interfaces, overall strength that can be tuned with mechanical confinement, geometrical hardening that increases the resistance to sliding along certain directions, and interlocking of the grains along certain loading directions. To produce mechanical confinement, we used a flexible vacuum bag, which enabled a controlled and constant hydrostatic pressure. In the future, stiffer modes of confinement

could be conceived to magnify the interlocking mechanisms further, for example, by using stiffer and/or prestretched vacuum bags, or stiff confining structures creating confinements along specific directions. It may then be possible for these granular crystals to approach the strong topological interlocking produced in topologically interlocked panels. These granular crystals also borrow some concepts and methods from granular mechanics such as granular crystallization, triaxial compression loading, and pressure-dependent yielding. The mechanics of these granular crystals are however markedly different from regular granular materials. They deform by controlled slip or by buckling instead of shear banding, they are highly anisotropic, and the traditional Mohr–Coulomb failure criterion is not applicable. Interestingly, the geometry of the individual grains completely governs the type of crystal that is obtained by vibrations as well as the anisotropy and strength of the granular crystal. How grain shape can be systematically varied to manipulate these emerging characteristics is an interesting question that will require further investigations. Our results also show that large numbers of grains can be crystallized and templated in a rectangular vibration box. How the shape of the box and the vibration patterns can be tuned to create crystals with other shapes and textures and/or with larger number of grains remains an open question. Defects such as vacancies, dislocations, or grain boundaries may also be introduced to increase strength further. Irregularities or gradients may also be beneficial to overall mechanical performance (25), although this aspect will also require further research. In addition, enrichments of the surface of the grains with controlled roughness, surface functionalization, or even the addition of soft adhesives at the interfaces may open even more alleys for mechanical tunability and programmability. We envision that these granular crystals could be used as modular structural materials that could be built from “universal” building blocks and that could be easily repaired, reshaped or altered on-site, with building blocks that can be recycled an indefinite number of times. Since the inelastic deformations of these materials rely on frictional contact, these materials could also be used for impact protection or energy dissipation. The extreme anisotropy of these crystals could also be exploited, for example, by shaping the crystal using the “malleable” plastic directions, for applications where loading is predominantly along one of the “strong” directions of the crystal. Finally, these granular crystals may also be used as “model materials” to explore and better understand atomic scale deformation mechanisms, which cannot be captured by traditional colloidal crystals models (26, 27). These could include mechanics of covalent crystal with strong directionality (28, 29), or unusual crystal plasticity that includes pressure-dependent and non-Schmid effects (30).

Methods

Details of compressive tests, grain-on-grain friction experiments, image tracking algorithm, and derivation of crystal plasticity model can be found in *SI Appendix*.

Data, Materials, and Software Availability. All study data are included in the article and/or *SI Appendix*.

ACKNOWLEDGMENTS. This work was sponsored by the University of Colorado Boulder and by the Army Research Office under Grant Number W911NF-21-1-0175. The views and conclusions contained in this document are those of the authors and should not be interpreted as representing the official policies, either expressed or implied, of ARO or the US Government. The US Government is authorized to reproduce and distribute reprints for Government purposes notwithstanding any copyright notation herein.

1. K. Bertoldi, V. Vitelli, J. Christensen, M. van Hecke, Flexible mechanical metamaterials. *Nat. Rev. Mater.* **2**, 170666 (2017).
2. A. Y. Dyskin, Y. Estrin, A. J. Kanel-Belov, E. Pasternak, Topological interlocking of platonic solids: A way to new materials and structures. *Philos. Mag. Lett.* **83**, 197–203 (2003).
3. T. Siegmund, "Heterogeneous topologically interlocked materials: A new class of heterogeneous materials" in *Advances in Heterogeneous Material Mechanics*, J. H. Fan, J. Q. Zhang, H. B. Chen, Z. H. Jin, Eds. (Desteck Publications Inc., Lancaster, PA, 2011), pp. 1124–1125.
4. M. Mirkhalaf, T. Zhou, F. Barthelat, Simultaneous improvements of strength and toughness in topologically interlocked ceramics. *Proc. Natl. Acad. Sci. U.S.A.* **115**, 9128–9133 (2018).
5. T. Siegmund, F. Barthelat, R. Cipra, E. Habtour, J. Riddick, Manufacture and mechanics of topologically interlocked material assemblies. *Appl. Mech. Rev.* **68**, 040803–040803 (2016).
6. A. Bahmani, J. W. Pro, F. Hannard, F. Barthelat, Vibration-driven fabrication of dense architected panels. *Matter* **5**, 899–910 (2022).
7. Z. Q. Wang, P. Song, F. Isvoranu, M. Pauly, Design and structural optimization of topological interlocking assemblies. *Acm Trans. Graph.* **38**, 1–13 (2019).
8. Y. Estrin, V. R. Krishnamurthy, E. Akleman, Design of architected materials based on topological and geometrical interlocking. *J. Mater. Res. Technol.* **15**, 1165–1178 (2021).
9. H. M. Jaeger, S. R. Nagel, R. P. Behringer, Granular solids, liquids, and gases. *Rev. Mod. Phys.* **68**, 1259–1273 (1996).
10. R. P. Behringer, B. Chakraborty, The physics of jamming for granular materials: A review. *Rep. Prog. Phys.* **82**, 012601 (2018).
11. F. Radjai, J.-N. Roux, A. Daouadi, Modeling granular materials: Century-long research across scales. *J. Eng. Mech.* **143**, 04017002 (2017).
12. G. Y. Onoda, E. G. Liniger, Random loose packings of uniform spheres and the dilatancy onset. *Phys. Rev. Lett.* **64**, 2727–2730 (1990).
13. R. P. Behringer *et al.*, Statistical properties of granular materials near jamming. *J. Stat. Mech.* **2014**, P06004 (2014).
14. E. Hascoet, H. J. Herrmann, V. Loreto, Shock propagation in a granular chain. *Phys. Rev. E* **59**, 3202–3206 (1999).
15. C. Daraio, V. F. Nesterenko, E. B. Herbold, S. Jin, Energy trapping and shock disintegration in a composite granular medium. *Phys. Rev. Lett.* **96**, 4 (2006).
16. M. A. Porter, P. G. Kevrekidis, C. Daraio, Granular crystals: Nonlinear dynamics meets materials engineering. *Phys. Today* **68**, 44–50 (2015).
17. Y. F. Wang, L. C. Li, D. Hofmann, J. E. Andrade, C. Daraio, Structured fabrics with tunable mechanical properties. *Nature* **596**, 238–243 (2021).
18. E. Brown *et al.*, Universal robotic gripper based on the jamming of granular material. *Proc. Natl. Acad. Sci. U.S.A.* **107**, 18809–18814 (2010).
19. A. G. Athanassiadis *et al.*, Particle shape effects on the stress response of granular packings. *Soft Matter* **10**, 48–59 (2014).
20. F. X. Villarruel, B. E. Lauderdale, D. M. Mueth, H. M. Jaeger, Compaction of rods: Relaxation and ordering in vibrated, anisotropic granular material. *Phys. Rev. E* **61**, 6914–6921 (2000).
21. L. K. Roth, H. M. Jaeger, Optimizing packing fraction in granular media composed of overlapping spheres. *Soft Matter* **12**, 1107–1115 (2016).
22. P. F. Damasceno, M. Engel, S. C. Glotzer, Predictive self-assembly of polyhedra into complex structures. *Science* **337**, 453–457 (2012).
23. J. Henzie, M. Grünwald, A. Widmer-Cooper, P. L. Geissler, P. Yang, Self-assembly of uniform polyhedral silver nanocrystals into densest packings and exotic superlattices. *Nat. Mater.* **11**, 131–137 (2012).
24. K. Iwashita, M. Oda, *Mechanics of Granular Materials: An Introduction* (CRC Press, 1999).
25. D. Y. Kim, T. Siegmund, Mechanics and design of topologically interlocked irregular quadrilateral tessellations. *Mater. Design* **212**, 110155 (2021).
26. P. Schall, I. Cohen, D. A. Weitz, F. Spaepen, Visualization of dislocation dynamics in colloidal crystals. *Science* **305**, 1944–1948 (2004).
27. E. Maire, E. Redston, M. P. Gulda, D. A. Weitz, F. Spaepen, Imaging grain boundary grooves in hard-sphere colloidal bicrystals. *Phys. Rev. E* **94**, 9 (2016).
28. C. Liu, X. Q. Song, Q. Li, Y. M. Ma, C. F. Chen, Smooth flow in diamond: Atomistic ductility and electronic conductivity. *Phys. Rev. Lett.* **123**, 6 (2019).
29. M. I. Eremets *et al.*, The strength of diamond. *Appl. Phys. Lett.* **87**, 3 (2005).
30. P. Steinmann, E. Kuhl, E. Stein, Aspects of non-associated single crystal plasticity: Influence of non-Schmid effects and localization analysis. *Int. J. Solids Struct.* **35**, 4437–4456 (1998).